PCCP

Accepted Manuscript

This is an *Accepted Manuscript*, which has been through the Royal Society of Chemistry peer review process and has been accepted for publication.

Accepted Manuscripts are published online shortly after acceptance, before technical editing, formatting and proof reading. Using this free service, authors can make their results available to the community, in citable form, before we publish the edited article. We will replace this *Accepted Manuscript* with the edited and formatted *Advance Article* as soon as it is available.

You can find more information about *Accepted Manuscripts* in the **Information for Authors**.

Please note that technical editing may introduce minor changes to the text and/or graphics, which may alter content. The journal's standard **Terms & Conditions** and the **Ethical guidelines** still apply. In no event shall the Royal Society of Chemistry be held responsible for any errors or omissions in this *Accepted Manuscript* or any consequences arising from the use of any information it contains.

Isolating the Spectral Signature of H_3O^+ in the Smallest Droplet of Dissociated HCl Acid

John S. Mancini[*] and Joel M. Bowman

The centrally important role of acids in aqueous chemistry has stimulated the search for the smallest droplet of hydrochloric acid. Based on several independent quantum calculations, this appears to be the $HCl(H_2O)_4$ cluster, which dissociates to the so-called solvent ion pair (SIP), $H_3O^+(H_2O)_3Cl^-$. Experimental verification of this prediction via infra-red spectroscopy is a major challenge and despite several recent reports of this SIP, there remains uncertainty about these observations. In this Report, we present a calculation of the IR spectrum of the SIP in a fashion that isolates the contribution from the signature hydronium ion, H_3O^+. The computed spectrum indicates that the vibrational states of the H_3O^+ are highly mixed, resulting in dispersed spectral features between 1300 and 3000 cm^{-1}, with the region between 2100 and 2900 cm^{-1} being especially rich. These predictions point out the complexity of the SIP spectrum and offer guidelines for experiment. The energy of the HCl fundamental for three minima of the undissociated $HCl(H_2O)_4$ cluster are also reported.

Fundamental studies of acids in biological and chemical contexts are obviously of great and intense interest.[1–5] Recent research has focused on basic questions, such as how many water molecules are required for acid formation, i.e., dissociation, to be favored over undissociated states.[6–12] The answer is typically sought by the detecting the presence or absence of signature spectral features of the hydrated proton in the infrared. These signatures are a matter of current high interest not only in acids but in closely related contexts, such as the purely hydrated H^+ with no negative counter ion. In the latter, the fundamental question is whether the hydration state is of the Eigen form, H_3O^+, or the Zundel form, $H_5O_2^+$, where the proton is bridged between two water molecules. In both areas of research, IR spectroscopy has been the dominant experimental tool; however, the interpretation of the measured spectra are a major challenge. This has been been highlighted for the vibrations of H^+ ions embedded in molecular clusters[6,13–19] and most recently for the $H^+(H_2O)_{21}$ cluster.[20]

Acid clusters, such as hydrated HCl, arguably present even greater challenges for the interpretation of the IR spectrum than hydrated H^+ clusters, while still sharing aspects in common. The majority of experimental studies of hydrated HCl have focused on small $(HCl)_m(H_2O)_n$ clusters, in which HCl is not dissociated to an ion pair. In these

cases the IR spectroscopy focuses predominantly on the HCl monomer stretch.[21–30] We recently reported anharmonic vibrational calculations of the energies of fundamental excitations of HCl in mixed clusters, $HCl(H_2O)$, $(HCl)_2(H_2O)$, $HCl(H_2O)_2$, $(HCl)_3(H_2O)$, $(HCl)_2(H_2O)_2$, and $(HCl)(H_2O)_3$, using *ab initio* many-body potentials, and obtained very good with agreement with experiment.[31]

From a number of independent theoretical studies, consensus has been reached that for $HCl(H_2O)_4$, among the several minima, the dissociated configuration, $H_3O^+(H_2O)_3 Cl^-$, is the most stable one.[32–37] This configuration is denoted as a solvent-ion-pair (SIP) conformation with C_3 symmetry. Numerous path integral and classical dynamical studies of this and larger ionized clusters have been reported.[38–42] Experimental IR spectroscopy studies of the $HCl(H_2O)_4$ cluster in superfluid He nanodroplets at below 1 K reported evidence of the SIP, based on two spectral features at around 2670 cm^{-1} and theoretical support[30,43] The peaks were assigned using scaled harmonic frequencies to the symmetric stretch of the H_3O^+ in two nearly isoenergetic SIP conformations.[43] However, the peak location and spectral line shape are nearly identical to those of the HCl stretch of the undissociated $(HCl)_2(H_2O)_2$ cluster.[30,44] In addition, Møller-Plesset perturbation theory (MP2) harmonic calculations, the most sophisticated level of theory applied to the SIP to-date, obtain the symmetric stretch at $\sim$2900 cm^{-1}, clearly in disagreement with the previous calculations.[30,44] Furthermore, it is unclear whether the kinetic energy needed to surmount the barriers to transition from undissociated configurations to the SIP configuration are accessible in the helium droplets where experi-

Cherry L. Emerson Center for Scientific Computation and Department of Chemistry, Emory University, Atlanta, GA 30322
[*]*E-mail: john.mancini@emory.edu*

ments took place.[45]

Motivated by both the central importance of the HCl(H$_2$O)$_4$ cluster and the uncertainty in the experimental evidence for its dissociation, we performed a calculation of the IR spectrum of the signature H$_3$O$^+$ ion in the SIP configuration. Consideration of coupling in the full cluster, which has thirty-six vibrational degrees-of-freedom, is far too large for rigorous quantum calculations and so we used the Local Monomer approach (LMon).[46,47] This is the approach that was applied successfully to the undissociated HCl clusters mentioned above.[31] In the application to HCl(H$_2$O)$_4$, the LMon approach is expanded to consider coupling among the twelve vibrational degrees-of-freedom (six intramolecular and six intermolecular) of H$_3$O$^+$ embedded in the H$_3$O$^+$(H$_2$O)$_3$ Cl$^-$ cluster shown in Fig. 1. The calculations make use of an *ab initio*-based potential energy surface, built from the highest quality electronic structure methods feasible and coupled-anharmonic vibrational calculations. The results indicate that the SIP spectrum is more complex than ones based on previously reported harmonic analyses.[30,33,37,43,44] Before presenting this spectrum, a brief description of the LMon method, potential and dipole moment surfaces is given next.
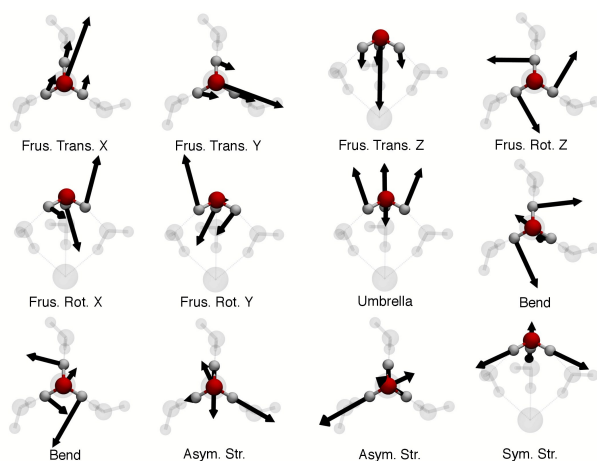
Fig. 1 Representations of the 12 LMon eigenvectors for the H$_3$O$^+$ embedded in the SIP cluster. The first six modes refer to intermolecular motions and the last six intramolecular motions. The abbreviations used are Frus. = Frustrated, Trans. = Translation, Rot. = Rotation, Sym = Symmetric, Asym = Asymmetric, Str. = Stretch. The labels, X, Y, Z are used to refer to the relative axis of the mode, where the Z-axis passes through the Cl$^-$ and the O of the H$_3$O$^+$.

The LMon potential energy surface (PES) describes the motion of H$_3$O$^+$ embedded in the SIP cluster, with fixed positions for the three H$_2$O monomers and the Cl$^-$. The equilibrium configuration of this cluster was determined by a full-dimensional geometry optimization, using Coupled Cluster Singles Doubles and Perturbative Triples excitations

(CCSD(T)), explicit correlation (-F12)[48] and the augmented correlation consistent double zeta basis (aVDZ).[49] At this configuration the LMon PES is given by

$$V = V_{H_3O^+} + V_{H_3O^+Cl^-} + \sum_{i=1}^{3} V_{H_3O^+H_2O(i)}$$
$$+ \sum_{i<j}^{3} V_{H_2O(i)(H_3O^+)H_2O(j)} + \sum_{i=1}^{3} V_{H_3O^+(Cl^-)H_2O(i)}, \quad (1)$$

where the terms are as follows. $V_{H_3O^+}$ is the potential of the isolated H$_3$O$^+$ monomer, which describes the six intramolecular vibrational degrees-of-freedom. $V_{H_3O^+Cl^-}$ is the twelve degree-of-freedom intrinsic two-body potential of H$_3$O$^+$ interacting with the fixed-position Cl$^-$, where the additional six degrees-of-freedom describe the H$_3$O$^+$ intermolecular modes. The meaning of the remaining terms in Eq. 1 follow the description of the $V_{H_3O^+Cl^-}$ and should be obvious. Each potential is a full-dimensional permutationally invariant linear-least squares fit to tens of thousands of electronic energies.[50,51] The one- and two-body interaction energies used for the fits were computed using CCSD(T) with the augmented correlations consistent triple zeta (aVTZ) basis or higher. These levels of theory are not computationally feasible for the three-body interactions and so CCSD(T)-F12/aVDZ energies were used. The higher-body interactions are neglected in the LMon PES, as they contribute less than 1% of the total cluster interaction energy.[35] Details about the basis sets and fits for the interaction potentials are given in the Supplementary Information (SI).

The LMon dipole moment surface (DMS) was generated in a similar manner to the LMon PES. It consists of one- and two-body dipole moments obtained from fits to MP2/aVTZ calculations. Details of these calculations and the fits are given in the SI.

The code MULTIMODE was used to obtain the embedded, 0 K, H$_3$O$^+$ IR spectrum employing the LMon PES and DMS. This code, in brief, performs vibrational configuration interaction (VCI) calculations using virtual states from a vibrational self-consistent field (VSCF) calculation to obtain eigenvalues and eigenfunctions of the Watson Hamiltonian.[52,53] Additional details of the MULTIMODE calculations are provided in the SI.

Before discussing the IR spectrum, we present numerical validation of the approach taken. This is done by examining harmonic frequencies and double harmonic intensities computed for the SIP cluster using various methodologies; these are given in Table 1. First, to test the accuracy of the LMon approach, results from a full harmonic normal-mode analysis (thirty-six degrees-of-freedom) and a LMon harmonic normal-mode analysis, both performed using MP2/aVDZ, are given in columns one and two of Table 1. As seen, they are in good agreement with each other for the 12 LMon modes. The av-

erage percent difference between the full and LMon approach is 9%, with the six highest frequencies differing by no-more than a 1% on average. Similar agreement is observed for the intensities in the two approaches. While the values in this test were computed with MP2/aVDZ, similar differences between full and LMon results are to be expected for subsequent higher level calculations. A full dimensional normal-mode analysis using CCSD(T) was not feasible for us, due to the huge computation time required. However, a LMon normal-mode analysis using CCSD(T)-F12/aVDZ was performed and the results are reported in column three of Table 1. Comparison of the *ab initio* to the LMon PES frequencies, shown in column four of Table 1, provide a semi-quantitative measure of the LMon PES quality. The comparison is not exact because of differences in the potentials and the configuration with which the analyses were applied. The LMon PES uses higher quality basis sets for the one- and two-body interactions, which constitute 90% of the total energy. Furthermore, the LMon PES lacks the unphysical effects of basis set superposition error, which are present in the direct calculation.[54] The differences in the direct *ab initio* and LMon PES energetics result in small (~ 0.01 Å) geometric differences in the minimum energy structure of the embedded H_3O^+. The optimized structure parameters of H_3O^+ from the *ab initio* and LMon PES are reported in the SI. The frequencies from the LMon PES values differ by less that 7% from the direct LMon CCSD(T)-F12/aVDZ calculations. While some of these differences may be the result of fitting errors or the lack of higher-body effects, they are more likely the results of a more accurate description of one and two-body interactions in the LMon PES . As a result, we consider the LMon results to be the benchmark values.

Table 1 Harmonic frequencies (cm^{-1}) and normalized double harmonic intensities of the embedded H_3O^+ in the SIP configuration computed using the different approaches.

| | Full MP2/aVDZ | | Local MP2/aVDZ | | Local CCSD(T)-F12/aVDZ | | Local LMon PES | |
Modes	Freq.	Inten.	Freq.	Inten.	Freq.	Inten.	Freq.	Inten.
Frust. Trans. X	328	14	238	3	236	3	228	0
Frust. Trans. Y	329	14	239	3	236	3	228	0
Frust. Trans. Z	392	1	306	1	305	1	303	0
Frust. Rot. Z	840	0	804	0	797	0	794	0
Frust. Rot. Y	979	6	873	0	890	0	913	0
Frust. Rot. X	979	6	874	0	891	0	913	0
Umbrella	1489	36	1469	23	1475	26	1399	37
Bend	1758	2	1748	2	1781	2	1889	1
Bend	1758	2	1749	2	1781	2	1889	1
Asym. Str.	2649	100	2665	100	2713	100	2803	100
Asym. Str.	2650	100	2667	100	2713	100	2803	100
Sym. Str.	2880	76	2881	50	2960	48	2957	71

The harmonic and coupled anharmonic IR spectra are shown in Fig. 2. In both spectra, the individual vibrational states are represented by sticks. Each stick was broadened with a Gaussian function of width 8 cm^{-1} to generate vibrational band shapes. Before discussing the greatly contrasting results, we note that the harmonic spectrum was computed nearly instantaneously, requiring less than 300 evaluations of
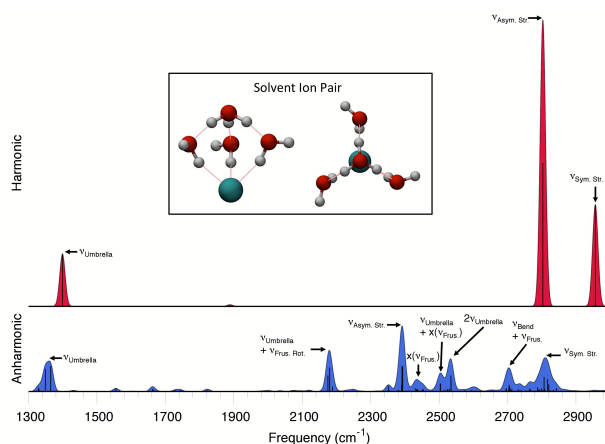
Fig. 2 Global minimum SIP configuration from two perspectives and its embedded H_3O^+ harmonic and coupled anharmonic spectrum. Each stick represents an individual state with the band shapes produced from the convolution of a Gaussians. The intensities of the two spectra are unscaled.

the LMon PES and the set-up and diagonalization of a 12×12 Hessian matrix. The calculation of the anharmonic spectrum required over a week of CPU time running serial on a workstation, with over five-million evaluations of the LMon PES and the set-up and diagonalization of the $26\,496 \times 26\,496$ VCI Hamiltonian matrix. This dichotomy in computational cost is mirrored in the resulting spectra. The harmonic spectrum is very simple, with only four harmonic states contributing to three significant features. In the anharmonic spectrum there are 206 IR active states from which eight individual Gaussian peaks were assigned. The eight peaks all have intensity greater than at least 10% of the largest Gaussian feature. Clearly the harmonic approximation is not suitable for characterizing the complexity of the embedded H_3O^+. The harmonic results in addition to failing to account for most of the H_3O^+ vibrational states, significantly overestimates the IR intensities of the features. The most intense anharmonic peak (891 km/mol) is less than a quarter of the harmonic spectrum's (3898 km/mol) most intense peak. Another interpretation of this "overestimation" of the intensities is that coupling "splinters" these large single peaks into many smaller dispersed ones. This is a common feature of complex spectra.[55]

In the anharmonic-coupled spectrum, each of the VCI state wavefunctions is heavily mixed, that is to say no single stick corresponds to "pure" fundamental or overtone. As a result of this strong mixing, we assigned the bands based on the dominant characteristics of the collection of VCI eigenstates from which they are formed. Details of this analysis are provided in SI. We complemented this analysis by comparing the peak positions to those computed by a separate, reduced-dimensional, calculation that involved only the six-highest frequency modes

of the H_3O^+. The result of the analysis of the eight spectral features is provided in Table 2, where the labels used in the Fig. 2 have been expanded upon.

Table 2 Quantum deconstruction of the IR spectrum of the SIP embedded H_3O^+. The sections *Reduced* and *Complete* refer to the results of the reduced-dimensional six-highest-frequency-mode coupled calculation and the full twelve-mode coupled calculation, respectively. The frequencies are reported in cm^{-1} and the intensities in normalized units. The column # of States indicates the number of VCI states in the band range

	Reduced	*Complete*			
	Peak	Peak	Band Range	Intensity	# of States
Umbrella	1367	1357	1300 - 1400	46	5
Umbrella + Frus. Rot. X/Y	-	2179	2150 - 2220	63	13
Asym. Str.	2458	2391	2370 - 2415	100	21
$2 \cdot$ Frus. Rot. Z + Frus. Rot. X/Y	-	2435	2415 - 2473	18	19
Umbrella + Frus. Tran. X/Y + Frus. Rot. X/Y	-	2500	2480 - 2515	25	15
$2 \cdot$ Umbrella	2569	2531	2515 - 2560	50	24
Bend + Frus. Rot.	-	2704	2680 - 2750	36	50
Sym. Str.	2778	2811	2750 - 2860	52	76

Numerous features in the VCI spectrum correspond to overtones and combination bands of the frustrated modes and umbrella motion which cannot be described using the standard double-harmonic approach. Many of these features, notably the band spanning 2415 - 2473 cm^{-1}, are characterized by several states that individually have small IR intensity. When the Gaussian convolution of these states with their neighbors is considered, bands with appreciable intensity are observed. The features, predominately in the range 2370 - 2860 cm^{-1} result from interactions among the stretching modes which lead to significant intensity sharing. The intensity sharing between the symmetric stretch and umbrella overtone is of particular note. In the VCI state analysis we observe that a Fermi resonance occurs between the symmetric stretch and umbrella overtone resulting in significant transfer of intensity from the symmetric stretch to the overtone. Outside the heavily mixed 2415 - 2473 cm^{-1} region there are two well defined peaks associated with the fundamental of the umbrella motion and combination bands of the umbrella + frustrated rotation.

Clearly, the spectral features of the SIP spectrum are complex, even after isolating the H_3O^+ features. Additional spectral features associated with the higher energy conformer of the SIP could also contribute to the observed experimental spectrum.[43] This alternate configuration is $\sim$200 cm^{-1} higher in energy and characterized by the rotation of one of the H_2O monomer's free OHs into a non-symmetric position. LMon CCSD(T)-F12/aVDZ harmonic stretch frequencies of this conformer shift as much as 47 cm^{-1} from the lower energy SIP conformation. While transitions between the higher energy structure and the ground state are unlikely, as a $\sim$400 cm^{-1} barrier must first be crossed, its formation in experimental studies alongside the lowest energy structure, could be possibility. Fortuitously, these features are outside the bulk of SIP H_3O^+ spectral signature, however, the do coincide with

the H_3O^+ combination bands of the umbrella + frustrated rotation. A visualization of this alternate configuration and its harmonic frequencies are reported in the SI.

Finally, there are three minima in the $HCl(H_2O)_4$ cluster that describe undissociated HCl. These three structures include a $HCl(H_2O)_3$ ring with a fourth water monomer accepting a single hydrogen-bond from the ring, a similar structure where the fourth water monomer donates and accepts a hydrogen-bond from the ring and a five-member ring. Visualizations of these structures are provided in the SI. The energies of these configurations relative to the SIP configuration (kcal) and their respective LMon HCl anharmonic frequencies (cm^{-1}) are: 6.0, 2093; 4.6, 2220; and 3.0, 2161. These HCl fundamental excitations are quite pure and so do not display the splintering that characterizes the embedded H_3O^+ spectrum. Thus, spectral features associated with these are at down-shifted from the main portion of the IR region of the SIP complex.

We anticipate that the complexity and diffuse nature of the H_3O^+ vibrational spectrum embedded in the SIP is not limited to this "smallest droplet of acid" but also occurs for embedded H_3O^+ in other systems. For example, both the $H^+(H_2O)_{21}$ and $H^+(H_2O)_4$ clusters broad spectra peaks were associated with embedded H_3O^+. The broad nature of these features are of note, considering they were performed at very cold temperatures. A possible explanation for this is the same anharmonic effects which cause the broad feature in the SIP cluster also occur for these systems as well. This, combined with delocalization of the free OH of the water monomers in these non-counter ion systems could result in reported line shapes. Further merit for this comparison comes from the report of a umbrella + frustrated rotation combination band in the $H^+(H_2O)_{21}$ similar to that reported here.[16]

Acknowledgements

References

1 J. Heberle, J. Riesle, G. Thiedemann, D. Oesterhelt and N. A. Dencher, *Nature*, 1994, **370**, 379–82.

2 M. H. B. Stowell, T. M. McPhillips, D. C. Rees, S. M. Soltis, E. Abresch and G. Feher, *Science*, 1997, **276**, 812–816.

3 D. Borgis and J. T. Hynes, *J. Phys. Chem.*, 1996, **100**, 1118–1128.

4 A. W. Omta, M. F. Kropman, S. Woutersen and H. J. Bakker, *Science*, 2003, **301**, 347–349.

5 K.-D. Kreuer, *Chem. Mater.*, 1996, **8**, 610–641.

6 K. R. Leopold, *Annu. Rev. Phys. Chem.*, 2011, **62**, 327–49.

7 F. M. Balci, N. Uras-Aytemiz, P. C. Gomez and R. Escribano, *Phys. Chem. Chem. Phys.*, 2011, **13**, 18145–18153.

8 D. K. Maity, *J. Phys. Chem. A*, 2013, **117**, 8660–8670.

9 B. Temelso, T. E. Morrell, R. M. Shields, M. A. Allodi, E. K. Wood,

K. N. Kirschner, T. C. Castonguay, K. A. Archer and G. C. Shields, *J. Phys. Chem. A*, 2012, **116**, 2209–2224.

10　P. Krishnakumar and D. K. Maity, *J. Phys. Chem. A*, 2014, **118**, 5443–5453.

11　K. Mizuse, N. Mikami and A. Fujii, *Angew. Chem. Int. Ed.*, 2010, **49**, 10119–10122.

12　M. Park, I. Shin, N. J. Singh and K. S. Kim, *J. Phys. Chem. A*, 2007, **111**, 10692–10702.

13　C.-K. Lin, C.-C. Wu, Y.-S. Wang, Y. T. Lee, H.-C. Chang, J.-L. KuoPresent address: School of Physi and M. L. Klein, *Phys. Chem. Chem. Phys.*, 2005, **7**, 938.

14　M. Okumura, L. I. Yeh, J. D. Myers and Y. T. Lee, *J. Chem. Phys.*, 1986, **85**, 2328.

15　G. E. Douberly, R. S. Walters, J. Cui, K. D. Jordan and M. A. Duncan, *J. Phys. Chem. A*, 2010, **114**, 4570–4579.

16　J. M. Headrick, E. G. Diken, R. S. Walters, N. I. Hammer, R. A. Christie, J. Cui, E. M. Myshakin, M. A. Duncan, M. A. Johnson and K. D. Jordan, *Science*, 2005, **308**, 1765–9.

17　A. B. McCoy, T. L. Guasco, C. M. Leavitt, S. G. Olesen and M. A. Johnson, *Phys. Chem. Chem. Phys.*, 2012, **14**, 7205–14.

18　T. C. Cheng, B. Bandyopadhyay, J. D. Mosley and M. A. Duncan, *J. Am. Chem. Soc.*, 2012, **134**, 13046–13055.

19　K. A. Servage, J. A. Silveira, K. L. Fort and D. H. Russell, *J. Phys. Chem. Lett.*, 2014, **5**, 1825–1830.

20　J. A. Fournier, C. J. Johnson, C. T. Wolke, G. H. Weddle, A. B. Wolk and M. A. Johnson, *Science*, 2014, **344**, 1009–12.

21　Z. Kisiel, B. A. Pietrewicz, P. W. Fowler, A. C. Legon and E. Steiner, *J. Phys. Chem. A*, 2000, **104**, 6970–6978.

22　M. Ortlieb, O. Birer, M. Letzner, G. W. Schwaab and M. Havenith, *J. Phys. Chem. A*, 2007, **111**, 12192–9.

23　B. S. Ault and G. C. Pimentel, *J. Phys. Chem.*, 1973, **77**, 57–61.

24　A. Schriver, B. Silvi, D. Maillard and J. P. Perchard, *J. Phys. Chem.*, 1977, **81**, 2095–2102.

25　A. J. Barnes, *J. Mol. Str.*, 1980, **60**, 343–346.

26　A. C. Legon and L. C. Willoughby, *Chem. Phys. Lett.*, 1983, **95**, 449–452.

27　C. Amirand and D. Maillard, *J. Mol. Str.*, 1988, **176**, 181–201.

28　M. Fárník, M. Weimann and M. A. Suhm, *J. Chem. Phys.*, 2003, **118**, 10120.

29　M. Weimann, M. FArnIk and M. A. Suhm, *Phys. Chem. Chem. Phys.*, 2002, **4**, 3933–3937.

30　M. Letzner, S. Gruen, D. Habig, K. Hanke, T. Endres, P. Nieto, G. Schwaab, L. Walewski, M. Wollenhaupt, H. Forbert, D. Marx and M. Havenith, *J. Chem. Phys.*, 2013, **139**, 154304.

31　J. S. Mancini and J. M. Bowman, *J. Phys. Chem. Lett.*, 2014, **5**, 2247–2253.

32　K. Andot and J. T. Hynes, *J. Mol. Liq.*, 1995, **64**, 25–37.

33　D. E. Bacelo, R. C. Binning and Y. Ishikawa, *J. Phys. Chem. A*, 1999, **103**, 4631–4640.

34　E. M. Cabaleiro-Lago, J. M. Hermida-Ramon and J. Rodrguez-Otero, *J. Chem. Phys.*, 2002, **117**, 3160.

35　A. Milet, C. Struniewicz, R. Moszynski and P. E. S. Wormer, *J. Chem. Phys.*, 2001, **115**, 349.

36　S. Odde, B. J. Mhin, S. Lee, H. M. Lee and K. S. Kim, *J. Chem. Phys.*, 2004, **120**, 9524–35.

37　S. Re, Y. Osamura, Y. Suzuki and H. F. Schaefer, *J. Chem. Phys.*, 1998, **109**, 973.

38　H. Forbert, M. Masia, A. Kaczmarek-Kedziera, N. Nair and D. Marx, *J. Am. Chem. Soc.*, 2011, **133**, 4062–72.

39　S. Sugawara, T. Yoshikawa, T. Takayanagi and M. Tachikawa, *Chem. Phys. Lett.*, 2011, **501**, 238–244.

40　L. Walewski, H. Forbert and D. Marx, *Chemphyschem*, 2013, **14**, 817–26.

41　Ł. Walewski, H. Forbert and D. Marx, *J. Phys. Chem. Lett.*, 2011, **2**, 3069–3074.

42　W. Lin and F. Paesani, *J. Phys. Chem. A*, 2013, **117**, 7131–7141.

43　A. Gutberlet, G. Schwaab, O. Birer, M. Masia, A. Kaczmarek, H. Forbert, M. Havenith and D. Marx, *Science*, 2009, **324**, 1545–8.

44　S. D. Flynn, D. Skvortsov, A. M. Morrison, T. Liang, M. Y. Choi, G. E. Douberly and A. F. Vilesov, *J. Phys. Chem. Lett.*, 2010, **1**, 2233–2238.

45　G. E. Douberly and R. E. Miller, *J. Phys. Chem. B*, 2003, **107**, 4500–4507.

46　Y. Wang and J. M. Bowman, *J. Chem. Phys.*, 2011, **134**, 154510.

47　J. S. Mancini and J. M. Bowman, *J. Chem. Phys.*, 2013, **139**, 164115.

48　G. Knizia, T. B. Adler and H.-J. Werner, *The Journal of Chemical Physics*, 2009, **130**, –.

49　T. H. Dunning, *The Journal of Chemical Physics*, 1989, **90**, 1007–1023.

50　B. J. Braams and J. M. Bowman, *Int. Rev. in Phys. Chem.*, 2009, **28**, 577–606.

51　A. Brown, A. B. McCoy, B. J. Braams, Z. Jin and J. M. Bowman, *J. Chem. Phys.*, 2004, **121**, 4105–4116.

52　J. M. Bowman, S. Carter and X. Huang, *Int. Rev. Phys. Chem.*, 2003, **22**, 533–549.

53　J. M. Bowman, T. Carrington and H.-D. Meyer, *Mol. Phys.*, 2008, **106**, 2145–2182.

54　A. Bende and S. Suhai, *Int. J. Quant. Chem.*, 2005, **103**, 841–853.

55　E. Kamarchik and J. M. Bowman, *J. Phys. Chem. Lett.*, 2013, **4**, 2964–2969.